JOURNAL OF MATERIALS RESEARCH AND TECHNOLOGY 2022;20:3579–3591

Available online at www.sciencedirect.com

jmr&t Journal of Materials Research and Technology

journal homepage: www.elsevier.com/locate/jmrt

Original Article

Preparation of new flexible antenna based on sol–gel synthesized $Mg_xCa_{(0.9-x)}Zn_{0.10}Fe_2O_4$ nanoparticle for microwave imaging applications

Md Atiqur Rahman [a,b], Mohammad Tariqul Islam [a,c,], Amran Hossain [a], Mandeep Jit Singh [a,*], Saleh Mohammad Albadran [c], Mohamed S. Soliman [d,e], Md Samsuzzaman [f,g]**

[a] *Department of Electrical, Electronic and Systems Engineering, Faculty of Engineering and Built Environment, Universiti Kebangsaan Malaysia, Malaysia*
[b] *Department of Electrical and Electronic Engineering, Faculty of Electrical and Electronic Engineering, Dhaka University of Engineering and Technology, Bangladesh*
[c] *Electrical Engineering Department, College of Engineering, University of Ha'il, Ha'il 81481, Saudi Arabia*
[d] *Department of Electrical Engineering, College of Engineering, Taif University, PO Box 11099, Taif 21944, Saudi Arabia*
[e] *Department of Electrical Engineering, Faculty of Energy Engineering, Aswan University, Aswan 81528, Egypt*
[f] *Dept. of Computer and Communication Engineering, Faculty of Computer Science and Engineering, Patuakhali Science and Technology, Patuakhali, Bangladesh*
[g] *Department of General Educational Development (GED), Faculty of Science and Information Technology (FSIT), Daffodil International University, Bangladesh*

ARTICLE INFO

Article history:
Received 21 May 2022
Accepted 20 August 2022
Available online 24 August 2022

Keywords:
Flexible antenna
Sol–gel synthesis
Nanoparticles
Tunable electromagnetic properties
Microwave head imaging

ABSTRACT

This article prepares, $Mg_xCa_{(0.90-x)}Zn_{0.10}Fe_2O_4$ nanoparticle-based new flexible microwave substrate materials to build flexible antennas. The $Mg_xCa_{(0.90-x)}Zn_{0.10}Fe_2O_4$ nanoparticles are synthesized using the sol–gel chemical method. There are three different weight percentages are chosen for "X" values i.e., X = 25%, 50%, and 75%. X-ray diffraction (XRD), field emission scanning electron microscopy (FESEM), and transmission electron microscopy (TEM) studies are used to evaluate the structural and morphological features of the produced nanoparticles. Dielectric Assessment Kit is also used to evaluate the nanoparticles' tunable dielectric characteristics (DAK). Loss tangents range from 0.00275 to 0.00675 while dielectric permittivity values range from 3.25 to 4.75. The magnetic characteristics of the produced samples are also investigated using the vibrating sample magnetometer (VSM). The Agilent 8501E module is used to calculate the adjustable magnetic permeability and magnetic loss tangent values. The magnetic permeability and magnetic loss tangent values obtained are in the range of 1.00–1.15 and 0.0035–0.0065, respectively. Later, a flexible antenna is designed on the prepared flexible substrate that operates within the frequency range of 1.60 GHz–3.00 GHz with a maximum gain of 5.15

* Corresponding author.
** Corresponding author.Department of Electrical, Electronic and Systems Engineering, Faculty of Engineering and Built Environment, Universiti Kebangsaan Malaysia, Malaysia.
E-mail addresses: tariqul@ukm.edu.my (M.T. Islam), mandeep@ukm.edu.my (M.J. Singh).
https://doi.org/10.1016/j.jmrt.2022.08.103

dBi. After that, this antenna is incorporated with a nine-antenna array-based portable microwave head imaging system. Finally, successful brain tumor detection is observed by post-processing the collected scattering parameters with an image reconstruction algorithm. The overall results ensure that the $Mg_xCa_{(0.90-x)}Zn_{0.10}Fe_2O_4$ nanoparticle-based new flexible microwave substrate materials can be a potential candidate for microwave head imaging and are suitable to fit with microwave devices.

1. Introduction

Flexible substrate materials are in high demand in modern microwave technology because they may be easily combined with uneven device surfaces without affecting functionality [1,2]. Flexible antennas, flexible metamaterials, flexible displays, flexible sensors, and health monitoring systems have all seen significant advancements in flexible technologies [3,4]. As a result, there has been a surge in interest in the synthesis and characterisation of crystalline spinel oxide materials in recent years [5,6]. Certain groups of spinel compounds show interesting magnetic, mechanical, catalytic, and electrical properties [7–9]. However, there are other classes of the transition metal oxides with the spinel structure including the spinel ferrites. All of them have both their advantages and their disadvantages. The iron spinels have excellent magnetodielectric properties also which discussed in different earlier works [10,11]. The basis for numerous technological applications of spinel oxides is related to their structural flexibility because various properties of these materials can be modified suitably by changing the chemical composition of the compound through cation redistribution or by substitution of a suitable dopant [12–14]. In the past, various crystalline spinel materials such as Mg-, Ca-, Co-, and Zn- ferrite-based spinel were attempted to dope with divalent and trivalent metal ions, and the effects of such substitutions on the structural, electric, and dielectric properties were reported [15–18]. The tunable electromagnetic properties have been observed, especially in ferrite-based spinel oxide materials that strongly depend on the dopant concentration. These substitutions can be used to derive a series of ferrites, which constitute a remarkable group of spinel compounds like: zinc ferrite, calcium-ferrite, cobalt ferrite, magnesium ferrite, manganese ferrite, zinc-nickel ferrite [19,20], zinc-calcium ferrite, zinc-cobalt ferrite, zinc-magnesium ferrite, zinc-manganese ferrite, etc. exhibiting fascinating physical behavior and thus provide possibilities for a wide range of practical applications [21]. Moreover, the ferrites also come in different types. For example, the existence of a magnetically ordered state and ferroelectric characteristics provides new opportunities for the widespread practical applications of hexaferrites [22,23]. Whereas, the ability to regulate these materials' magnetic characteristics is the vital point for introducing such applications. Besides, due to their immobilized characteristics, ferrite-based spinel's possess high electrical resistivity, low dielectric, and loss tangent. These properties allow them to be used as a dielectric material for microwave application devices [24,25].

Despite its many benefits, standard microstrip antennas have some drawbacks, including limited bandwidth, poor gain, and efficiency, as well as a relatively large size. Traditional antennas are usually made of rigid materials, whereas flexible antenna materials can be made of lightweight, thin, low-profile materials that can be easily placed on irregular surfaces [26–29]. As a result, a lot of effort is put into developing flexible materials that may be employed in compact metamaterial and antenna structures to achieve the necessary bigger bandwidth, high gain, higher efficiency, and superior radiation properties. The researchers have described a variety of flexible antennas, including paper-based, textile, fluidic, Kapton Polyimide, and natural rubber. Using the solid–state reaction technique (SSRT) and flexible polycrystalline LiTiMg ferrites substrate for an X band application resulted in a 37 percent reduction in antenna size when compared to dielectric substrates [30]. Some more different methods also used by the researchers for the synthesis of the precursor oxide compounds such as, the one-pot sol–gel autocombustion method and the pulsed laser ablation in liquid (PLAL) method [31,32]. A triangular microstrip patch antenna is devised and manufactured using LiTiZn polycrystalline substrate instead of dielectric substrates. Another intriguing discovery from this study was that employing ferrites as a substrate improved the dielectric substrate-based antenna's performance [33]. In order to reduce the size of the low-frequency antenna, a Ni–Cu–Zn ferrites substrate is also used [34]. Nickel ferrite has also been utilized to boost antenna bandwidth and reduce antenna size, which has been investigated [35]. An E-shaped microstrip patch antenna was created using a Dy-Sm-doped Mg-ferrite substrate that outperformed commercial materials [36]. Moreover, the use of ferrite-based flexible metamaterial and antenna are day by day increasing in the electronics products to meet their future demands in consumer electronics components, automotive, energy and power, medical imaging and healthcare, biomedical applications, and other related fields [37,38]. It is well known that the combination of different compounds which have excellent electronic properties leads to new composite materials which have earned great technological interest in recent years [39,40]. Nowadays, different categories of imaging technologies: computed tomography (CT) scanning, X-ray screening, magnetic resonance imaging (MRI), biopsy, positron emission tomography (PET), and ultrasound screening are used to diagnose brain tumors in modern medical healthcare facilities [41–44]. These existing imaging modalities help physicians and radiologists detect brain tumors and other health-related diseases. The major drawbacks of these imaging technologies are growing cancerous risk because of high dose radiation,

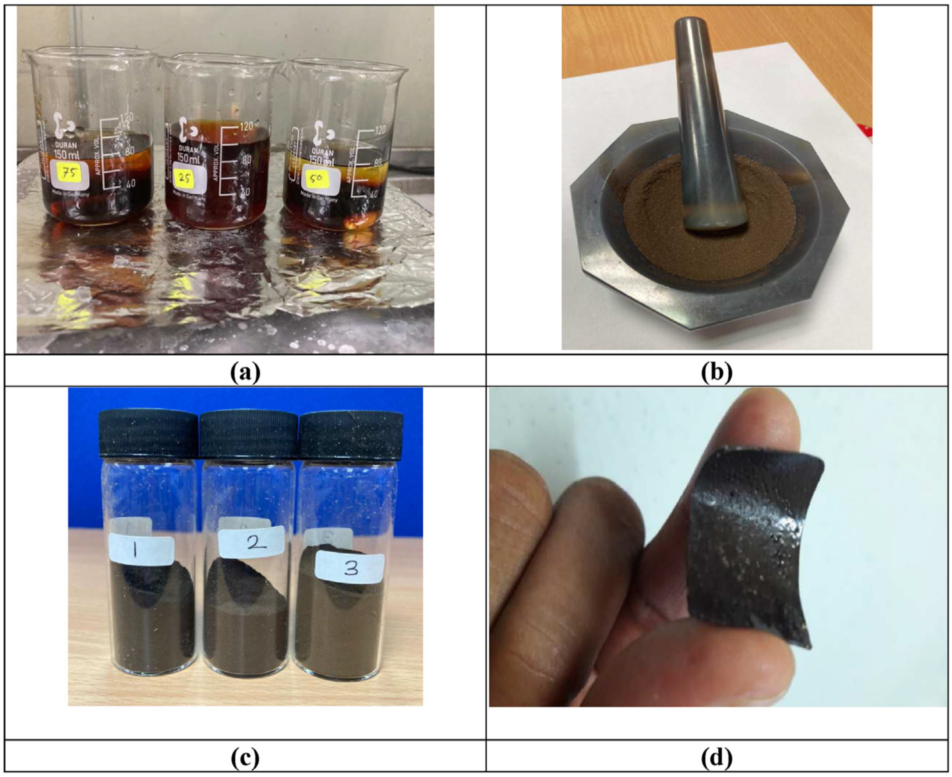

Fig. 1 – The synthesis steps of $Mg_xCa_{(0.90-x)}Zn_{0.10}Fe_2O_4$ nanoparticles and development of flexible substrate as well.

dangerous for pregnant women and old patients, high ionizing with brain cells, expensive, the risk for pacemaker and implantable cardioverter patients, time-consuming, and less susceptibility [41,42,44–50]. Microwave imaging research has been growing and showed excellent attention to the researchers for medical applications due to significant characteristics such as: cost-effective with a low profile, non-ionizing radioactivity, non-invasive, risk-free ionization with the tissues, low powered penetration capability, and safe for human body [41,47,48,50–56]. Recently, a microwave brain imaging (MBI) system has been utilized to identify the brain abnormalities such as brain tumors, cancer, stroke, and internal hemorrhage in the brain [47,51,54–56]. The MBI system consists of an antenna array, mechanical devices, and an image processing unit. The antenna is an essential piece of equipment, and its characteristics are a significant factor in producing the desired image. A single antenna transmits the microwave signals towards the region of interest, and receiver antenna(s) receive the backscattering signals. Different antennas have been offered to develop an MBI system to detect brain tumors.

In this study, sol–gel synthesized $Mg_xCa_{(0.90-x)}Zn_{0.10}Fe_2O_4$ nanoparticle-based flexible substrate material is developed to fabricate flexible antennas with three distinct X values (X = 25, 50, and 75). The XRD, FESEM, and TEM analysis are used to investigate the prepared ferrite-based nanoparticles' structural and morphological characteristics. The Dielectric Assessment Kit (DAK) and Vibrating Sample Magnetometer (VSM) are used to examine electromagnetic characteristics. The dielectric constant ranged from 3.25 to 4.75 and the loss tangents from 0.002 to 0.008. Whereas, the permeability values ranged from 1.00 to 1.15 and magnetic loss tangents from 0.0035 to 0.0065. Later, a wideband antenna is designed and manufactured on the suggested flexible substrate. The flexible antenna has a bandwidth of 1.5 GHz from 1.5 GHz to 3.00 GHz. After that, a nine-antenna array-based portable microwave head imaging system is built using the flexible antenna. The scattering parameters are acquired by introducing with and without tumor head phantoms into the system. Finally, the received signals are post-processed using the Iteratively Corrected Delay-Multiply-and-Sum (IC-DMAS) image reconstruction algorithm, and the brain tumor can be effectively recognized. The overall experiments verify that the proposed $Mg_xCa_{(0.90-x)}Zn_{0.10}Fe_2O_4$ nanoparticle-based novel flexible microwave substrates provide tunable electromagnetic characteristics and are ideal for building flexible antennas for microwave head imaging systems.

2. Material synthesis and flexible substrate preparation

First, $Mg_xCa_{(0.90-x)}Zn_{0.10}Fe_2O_4$ nanoparticles were synthesized using the sol–gel chemical process. Nearly similar materials also synthesized using the sol–gel method and found excellent tunable electromagnetic properties [31,32]. All raw ingredients, including magnesium nitrate, calcium nitrate, zinc nitrate, iron nitrate, and others, are bought in hydrate form

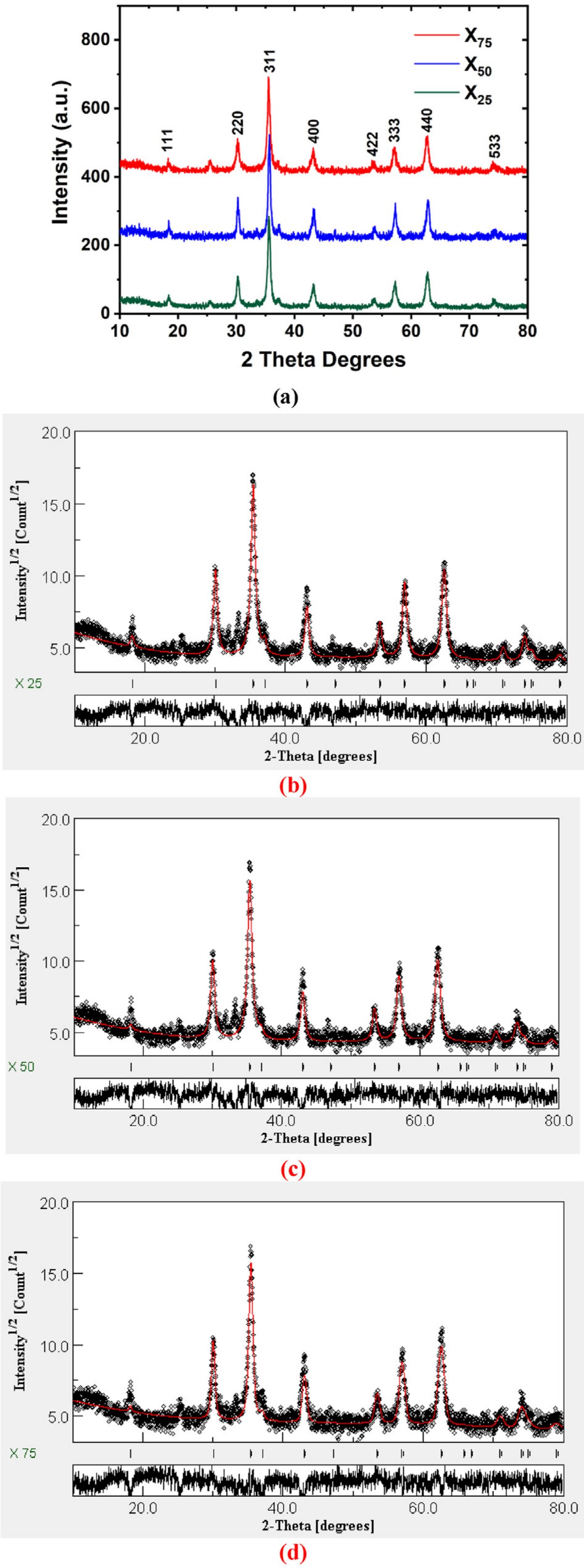

Fig. 2 – (a) Typical XRD pattern of $Mg_xCa_{(0.90\text{-}x)}Zn_{0.10}Fe_2O_4$ nanoparticles with different X values, and the plots obtained from MUAD program using Rietveld refinement for (b) X = 25, (c) X = 50, & (d) X = 75 respectively.

from SIGMA-ALDRICH, USA. A precision balance was used to weigh the needed amount of nitrates, which was then dissolved in 75 ml of distilling water according to the x values (x = 25, 50, 75) in a beaker. The beaker is put on top of a magnetic hot plate stirrer (Cimarec+TM Hotplate, Thermo Fisher Scientific) and swirled continuously at 90 °C to make a homogeneous solution. As a chelating agent, citric acid was also added to the solution. By evaporating some water, the solution becomes a crimson gel after 4 h, and the nitrates link together. The solutions were then dried in an oven for 1 h at 150 °C. The dried chemicals are then hand crushed with a marble mortar pestle. The pulverized powders were then transferred to crucible pots and calcined for 1 h at 800 °C in MTI Corporation's 1200C Muffle Furnace. As a result, MgxCa(0.90-x)Zn0.10Fe2O4 nanoparticles were created, and the flexible microwave substrates were created by mixing the nanoparticles with PVA glue at a ratio of 1 gm powder to 10 ml glue, as shown in Fig. 1(a–d).

3. Material characterization

3.1. X-ray diffractions (XRD) analysis

At first, by the typical X-ray diffractions (XRD) analysis the structural properties of the synthesized $Mg_xCa_{(0.90\text{-}x)}Zn_{0.10}Fe_2O_4$ nanoparticles were investigated and the XRD plots are illustrated in Fig. 2(a). The major peaks are located at (111), (220), (311), (400), (422), (333), (440), and (533) planes with reference patterns at PDF 01-080-6718 and PDF 01-086-4425. With the increasing value of X, the crystallinity has been improved, and the more sharper and thinner peaks are observed. This is because of the electronic properties for the complex oxides strongly depend on the average crystallite size and crystallite size distribution. This dependence is especially manifested for the mezzo- and nano-scale crystallites with a wide distribution spectrum [57,58]. The following equations results, which are shown in Table 1, were used to compute the crystalline dimension (D) and the lattice parameter (a) using the broadening peak of (311).

$$D = \frac{0.94\,\lambda}{\beta cos\theta} \quad (1)$$

$$n\ size a = d\sqrt{h^2 + k^2 + l^2}, \quad (2)$$

Where the symbols have their traditional significance.

In addition, the ionic coordinates and degree of inversion of the resulting spinel's are investigated from the X-ray or

Table 1 – The calculated crystalline size (*D*) and lattice constant (*a*) values of $Mg_xCa_{(0.90\text{-}x)}Zn_{0.10}Fe_2O_4$ nanoparticles with different X values.

X values (%)	*D* (nm)	*a* (Å)
25	17.90	5.650
50	16.43	5.630
75	14.97	5.617

Table 2 – Atom Site list of the prepared samples obtained from Rietveld refinement.

Sample	Atom	x	Y	z
X = 25	Mg	0.5	0.5	0.5
	Ca	0.5	0.5	0.5
	Zn	0.125	0.125	0.125
	Fe	0.125	0.125	0.125
	O	0.256	0.256	0.256
X = 50	Mg	0.5	0.5	0.5
	Ca	0.5	0.5	0.5
	Zn	0.125	0.125	0.125
	Fe	0.125	0.125	0.125
	O	0.267	0.267	0.267
X = 75	Mg	0.5	0.5	0.5
	Ca	0.5	0.5	0.5
	Zn	0.125	0.125	0.125
	Fe	0.125	0.125	0.125
	O	0.279	0.279	0.279

neutron diffraction data analysis by using the Rietveld method in the MUAD (Materials Analysis Using Diffraction) program [59,60]. The plots obtained from Rietveld refinement are demonstrated in Fig. 2(b–d) for X = 25, 50 and 75 respectively. Moreover, the Atom Site list of the prepared samples obtained from Rietveld refinement are tabulated in Table 2.

3.2. *Field emission scanning electron microscopy (FESEM) analysis*

Field Emission Scanning Electron Microscopy (FESEM) was used to examine the morphological properties of $Mg_xCa_{(0.90-x)}Zn_{0.10}Fe_2O_4$ nanoparticles. At a 1-μm magnification scale, Fig. 3 displays microscopic pictures of $Mg_xCa_{(0.90-x)}Zn_{0.10}Fe_2O_4$ nanoparticles. The particles are uniformly dispersed and have 14–18 nm of average grain size. The grain size was measured using the line intercept technique and showed good agreement with XRD analysis. Because of cation position distribution in the lattice, the grain changed as the X values changed.

3.3. *Transmission Emission Microscopy (TEM) analysis*

The synthesized $Mg_xCa_{(0.90-x)}Zn_{0.10}Fe_2O_4$ nanoparticles were also taken up through Transmission Emission Microscopy (TEM) analysis for further investigation of the phase structure and morphology. The TEM images are shown in Fig. 4 for the different X values of the prepared samples. According to TEM images, most of the nanoparticles had found in a spherical form having less thickness and with just a few elongated particles. It is also observed that with a lower concentration of X values the particles are found well-distanced. But the higher

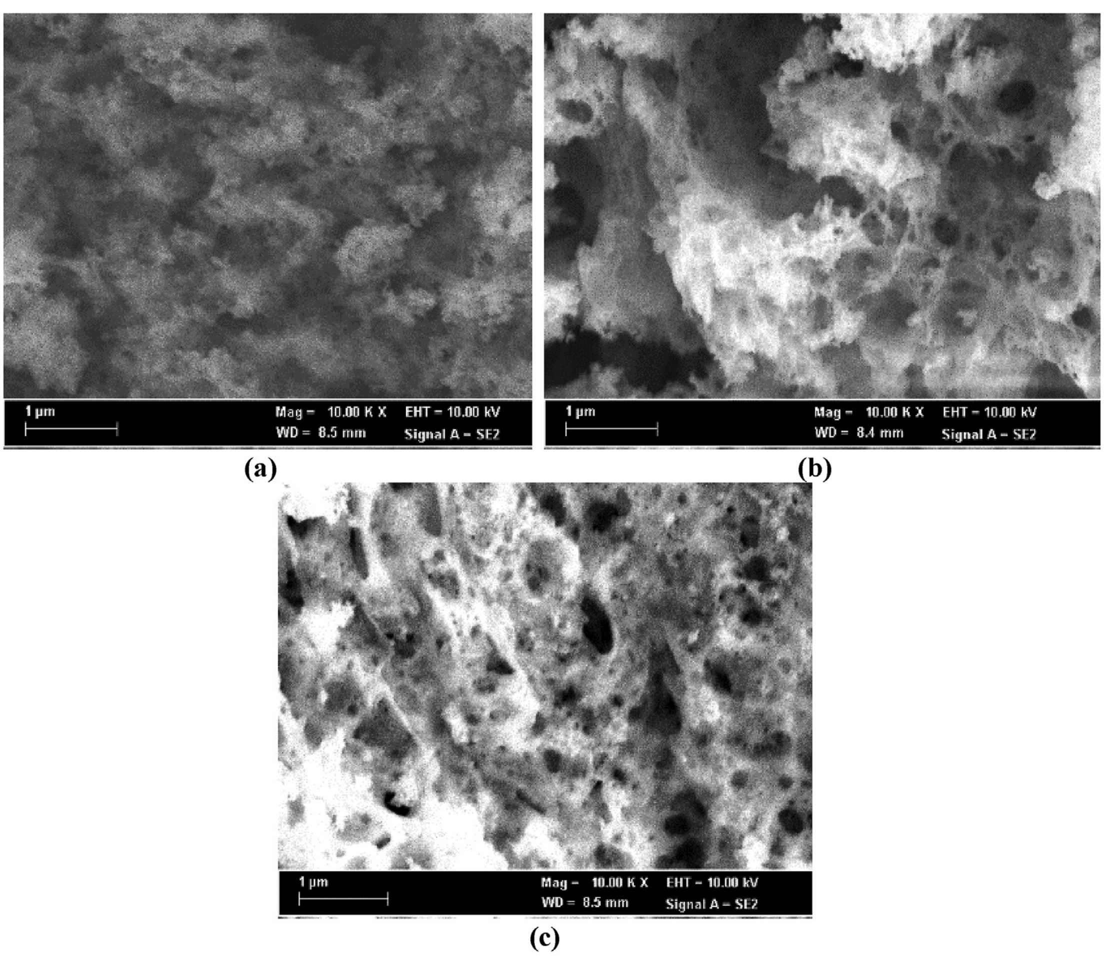

Fig. 3 – FESEM images of $Mg_xCa_{(0.90-x)}Zn_{0.10}Fe_2O_4$ nanoparticles with different X values.

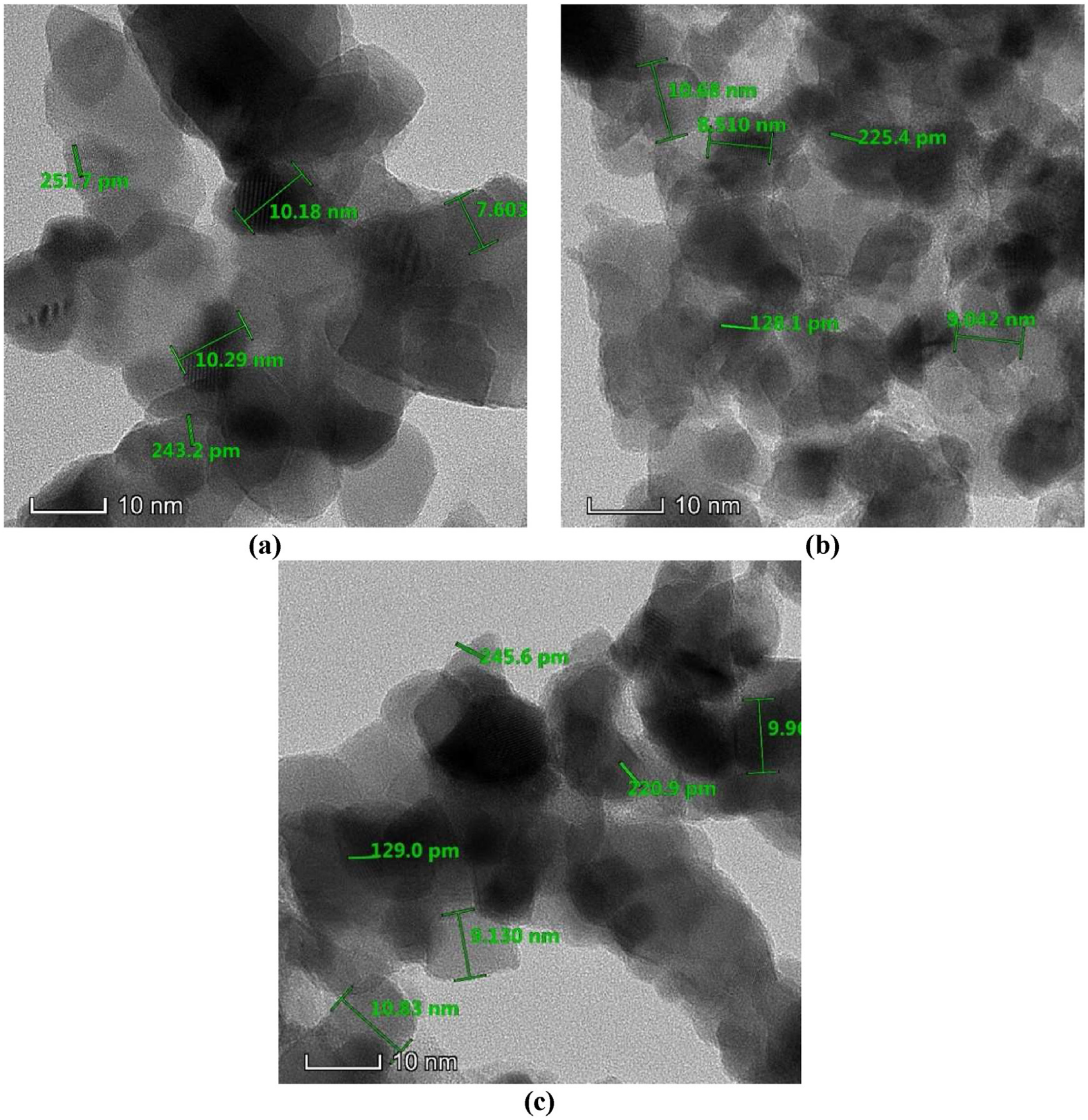

Fig. 4 – TEM images of $Mg_xCa_{(0.90-x)}Zn_{0.10}Fe_2O_4$ nanoparticles with different X values.

concentration of X values results in particle agglomeration due to magnetic interactions among nanoparticles. The particle size ranges between 14 and 18 nm as assessed by TEM images.

4. Electromagnetic analysis

4.1. *Dielectric analysis*

It is critical to understand the dielectric properties of the proposed $Mg_xCa_{(0.90-x)}Zn_{0.10}Fe_2O_4$ nanoparticles, such as dielectric constant and loss tangent, in order to test its microwave applicability. The dielectric evaluation kit evaluated the values of the dielectric constant and loss tangents of the prepared samples (DAK 3.5, SPEAG, Schmid & Partner Engineering AG). Fig. 5 shows a graphical representation of the dielectric constant and loss tangent values. Because of the differences in the materials compositions of the nanoparticles, the dielectric constant values range from 3.25 to 4.75, while the loss tangents range from 0.00275 to 0.00675. Due to conducting grain separations in porous ferrite samples, the values of the dielectric parameters show very minor changes [61], which also obeys Koop's phenomenological hypothesis and the Maxwell–Wagner model of interfacial polarization [62,63].

It is well known that the complex 3d-metal oxides easily allow the oxygen excess and/or deficit. Oxygen excess and deficit can increase and decrease the oxidation degree of 3d-metalls. The changing of charge state of 3d-metalls as a consequence of changing of oxygen content changes such electrical parameters as dielectric permittivity, dielectric loss tangent, conductivity, resistivity, as well as band gap. An increase in the unit cell parameter may be also due to oxygen deficiency [64,65]. Thus, the oxygen stoichiometry can be analyzed with the future materials. Overall, the produced $Mg_xCa_{(0.90-x)}Zn_{0.10}Fe_2O_4$ nanoparticles have tunable dielectric characteristics with flexible and could be a possibility for microwave applications, according to the findings.

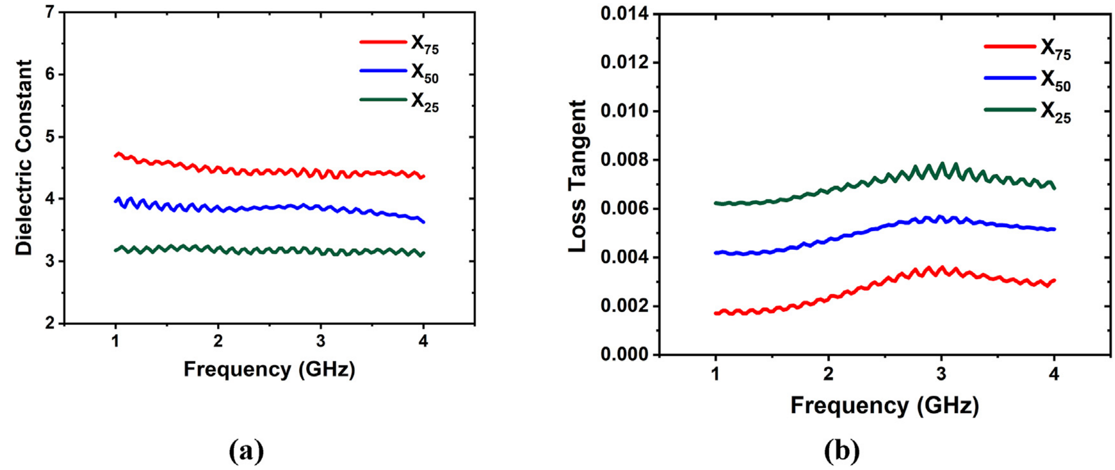

Fig. 5 – (a) Dielectric constant and (b) loss tangents of $Mg_xCa_{(0.90-x)}Zn_{0.10}Fe_2O_4$ nanoparticles with different X values.

4.2. *Magnetic properties analysis*

To verify the proposed $Mg_xCa_{(0.90-x)}Zn_{0.10}Fe_2O_4$ nanoparticles' microwave applicability, it is also very important to know their magnetic characteristics, such as the magnetization (M)-magnetic field (H) hysteresis loop, permeability, and magnetic loss tangent. The values of M (emu/g) and H (Oe) were determined using SQUID VSM and the plots are illustrated in

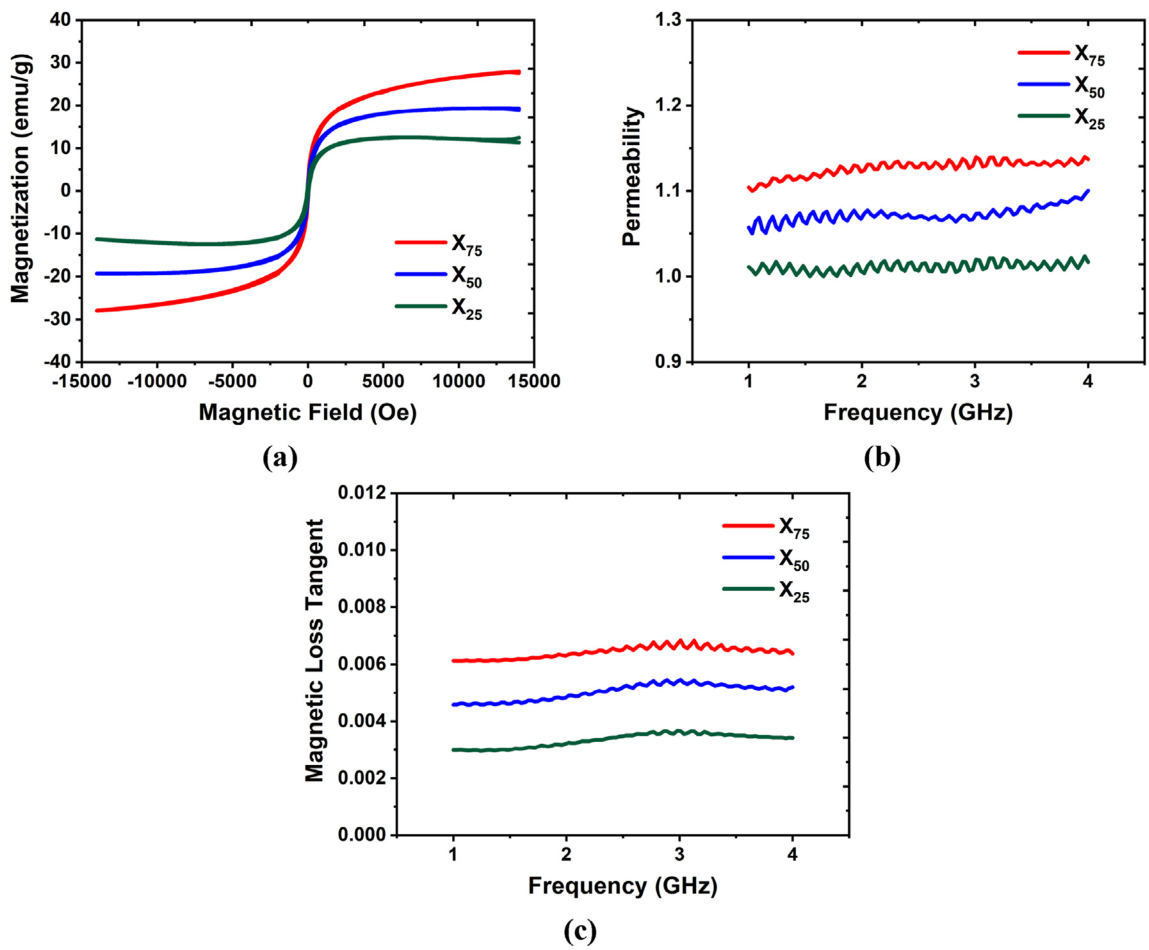

Fig. 6 – (a) M–H hysteresis, (b) permeability and (c) magnetic loss tangents of $Mg_xCa_{(0.90-x)}Zn_{0.10}Fe_2O_4$ nanoparticles with different X values.

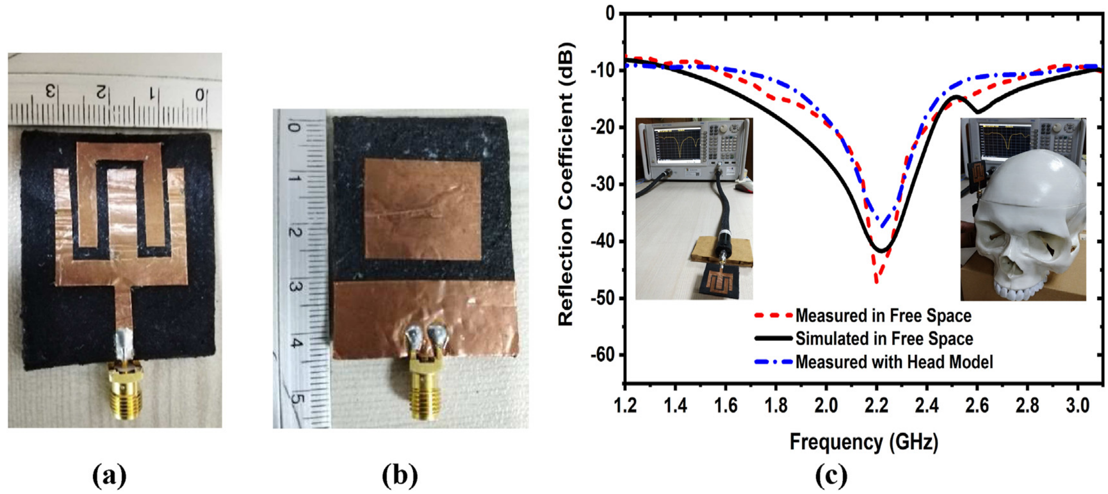

Fig. 7 – Fabricated antenna and reflection coefficient: (a) Top view, (b) back view, (c) Reflection coefficient.

Fig. 6(a). Moreover, the values of the permeability and magnetic loss tangent of the prepared samples were estimated by post-processing the scattering parameters S_{11} and S_{21} using the Agilent 85071E module [66,67]. Whereas, the scattering parameters S_{11} and S_{21} are collected from the vector network analyzer by placing the prepared substrate materials between two waveguides. The graphical illustration of the permeability and magnetic loss tangent values is presented in Fig. 6(a–b). The values of the permeability are varying from 1.00 to 1.15, whereas the values of the magnetic loss tangents are varying from 0.0035 to 0.0065. Due to the variation in the materials compositions of the nanoparticles, as it is well established by the researchers that the combination of different compounds which have excellent electronic properties leads to new composite materials which have earned great technological interest in recent years [39,40]. The magnetic properties of materials also found vary with the due to the oxygen deficiency [64,65]. The overall results also ensure that the synthesized $Mg_xCa_{(0.90-x)}Zn_{0.10}Fe_2O_4$ nanoparticles offer tunable magnetic properties and can be a potential candidate for microwave applications.

5. Application to microwave imaging

A wideband antenna operating in the frequency range of 1 GHz–4 GHz with high gain and directed radiation characteristics is required for microwave head imaging [54–56]. In this paper, a wideband antenna is designed and built on a flexible substrate based on MgxCa(0.90-x)Zn0.10Fe2O4 nanoparticles, and then measured to see if it meets the requirements for imaging. Fig. 7 depicts a constructed antenna prototype (a-b). The antenna's optimum dimensions are $40 \times 35 \times 1.6$ mm^3. The antenna's operational frequency ranges from 1.50 to 3.00 GHz, with a maximum gain of 5.15 dBi. The antenna is measured in free space and with the produced 3D head model to verify the performance for imaging purposes. Fig. 7 shows the manufactured antenna's reflection coefficient (c). The antenna demonstrated good agreement with the simulated outcome, as evidenced by the measured result. Using CST software, a Hugo head model is used to simulate the planned antenna and evaluate its performance. CST software is used to import the Hugo model. The many viewpoints of the simulation model are depicted in Fig. 8. Fig. 8 depicts a perspective view with a single

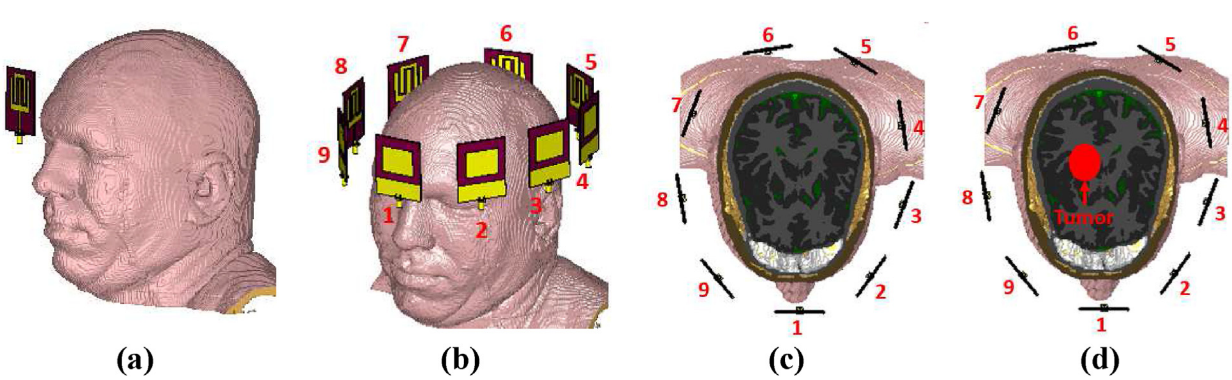

Fig. 8 – Simulated 3D Hugo head model: (a) perspective view with a single antenna, (b) Simulated nine antenna array setup, (c) Nine antenna set up without tumor (Healthy brain) (d) Nine antenna setup with tumor (Unhealthy brain).

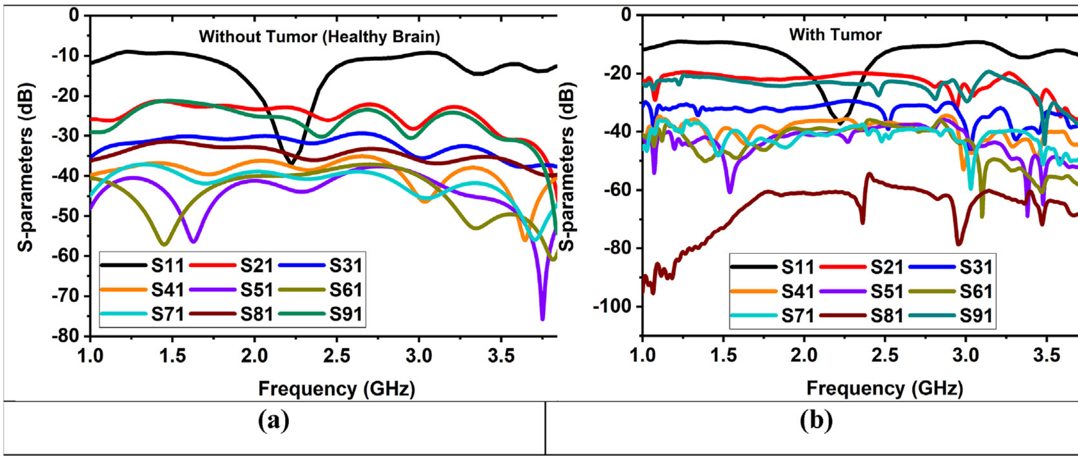

Fig. 9 – S-parameters: (a) without tumor, (b) with tumor.

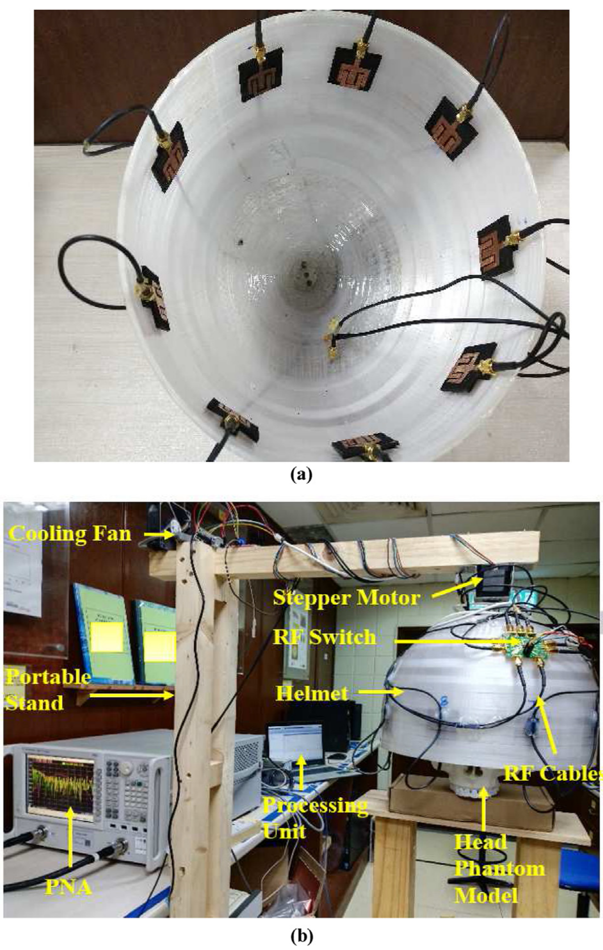

Fig. 10 – Overall head imaging system: (a) Nine antennae set up inside the helmet, (b) the Whole system.

antenna (a). Fig. 8(b–d) shows the simulation-based nine antenna array arrangement without tumor (healthy brain) and with tumor (unhealthy brain). Fig. 9 shows the S-parameters of the array setup with and without tumor. In the absence of the tumor inside the brain, the greatest resonance within the frequency band is −60 dB, as shown in Fig. 9(a). In contrast, the greatest resonance within the frequency range for the presence of the tumor inside the head with S-parameters modifications is −80 dB in Fig. 9(b). Initially, a four-layered 3D tissue-mimicking head phantom (DURA, CSF, white matter, and gray matter) with a tumor is fabricated. The tissues and tumors are fabricated according to the preparation process presented in [68]. Then, the tumor is placed at different positions in the fabricated phantom to investigate the imaging outcomes.

The overall head imaging system is shown in Fig. 10. The proposed system consists of flexible nine antenna arrays, a custom-made half-cut elliptical-shaped helmet, a stepper motor, a portable stand, RF switch, microcontroller, and a PNA E8358A transceivers. The stepper motor is attached to the portable stand, which rotates clockwise with a 7.2 angle at every step to cover the whole (360) area. The helmet is connected with the motor by the motor shaft. The diameter of the helmet is 250 mm. The antenna is attached inside the helmet by double-sided foam tape. The angular distance from the antenna to the antenna is 40 to cover the whole area of the system. The antenna position is set 100 mm up from the bottom point of the helmet to adjust the phantom head position. The PNA is connected to the computer through the GPIB port. Port A is connected to the transmitting antenna, and Port B is connected to the RF switch for receiving the backscattered signals. The fabricated 3D head phantom model is placed at the center position of the helmet to verify the system performance. The backscattered signals (i.e., S11, S21, S31, … S91) are collected by the PNA in each 7.2 rotation. Later, the collected signals are post-processed and utilized by the Iteratively Corrected Delay-Multiply-and-Sum

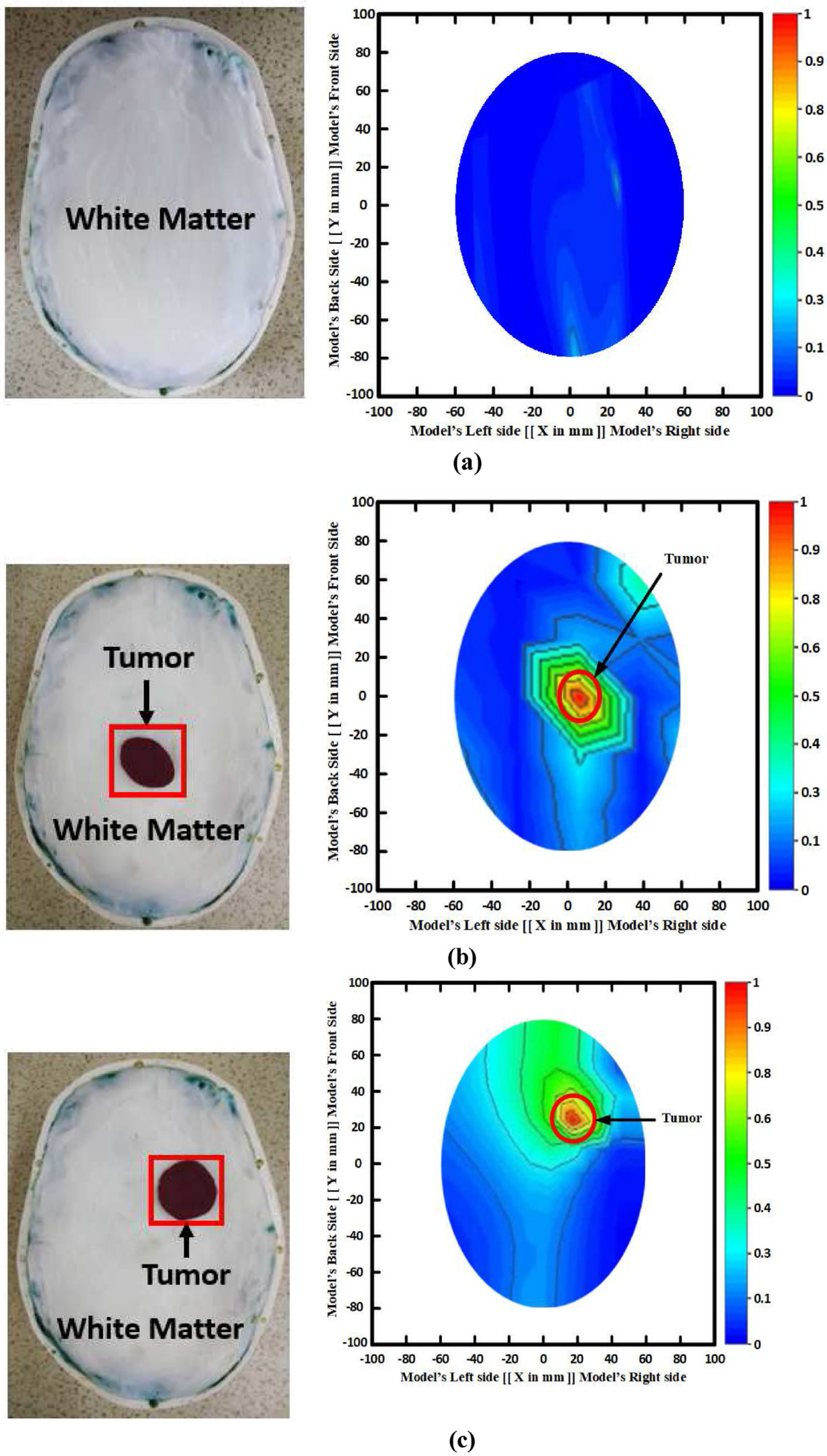

Fig. 11 – Fabricated phantom and reconstructed imaging results: (a) Image without tumor, (b–c) Image with a tumor at different positions.

(IC-DMAS) image reconstruction algorithm [69] to reconstruct the brain tumor images. The reconstructed brain images, including tumor, is presented in Fig. 11. Fig. 11(a) represents the non-tumor image (i.e., healthy brain), and Fig. 11(b–c) represents the single tumor image at different places respectively. The circular red mark in the images presents the tumor detection and position. It is concluded that the proposed implemented microwave head imaging system by the flexible antenna can identify the brain tumor with a location inside the brain. Therefore, the proposed $Mg_xCa_{(0.90-x)}Zn_{0.10}Fe_2O_4$ nanoparticles-based flexible antenna can be a suitable candidate to detect brain tumors in microwave head imaging applications.

6. Conclusion

In this article, sol–gel synthesized $Mg_xCa_{(1-x)}Zn_{0.10}Fe_2O_4$ nanoparticle-based flexible substrate material is prepared to build flexible antennas with three different X values (X = 25, 50, and 75). The structural and morphological properties of the proposed ferrite-based nanoparticles are characterized through XRD, FESEM, and TEM analysis. The tunable electromagnetic properties are investigated by Dielectric Assessment Kit (DAK) and Vibrating Sample Magnetometer (VSM). The dielectric constant values varied from 3.25 to 4.75 and loss tangents from 0.002 to 0.008. Whereas, the permeability values varied from 1.00 to 1.15 and magnetic loss tangents from 0.0035 to 0.0065. Later, a wideband antenna is designed and fabricated on the proposed flexible substrate. The flexible antenna offers a bandwidth of 1.5 GHz ranging from 1.5 GHz to 3.00 GHz. After that, a nine-antenna array-based portable microwave head imaging system is developed by utilizing the above flexible antenna. Then the scattering parameters are collected by placing with and without tumor head phantoms into the system. Finally, the collected signals are post-processed by the Iteratively Corrected Delay-Multiply-and-Sum (IC-DMAS) image reconstruction algorithm and it is observed that the brain tumor can be successfully detected by the whole setup. The overall investigations ensure that the proposed $Mg_xCa_{(1-x)}Zn_{0.10}Fe_2O_4$ nanoparticle-based new flexible microwave substrates offer tunable electromagnetic properties and are suitable for developing flexible antennas for microwave head imaging systems.

Declaration of competing interest

The authors declare that they have no known competing financial interests or personal relationships that could have appeared to influence the work reported in this paper.

Acknowledgement

This work is supported by the Ministry of Higher Education (MoHE), Malaysia research grant code: FRGS/1/2021/TK0/UKM/01/6.

REFERENCES

[1] Suguna S, Shankar S, Jaganathan SK, Manikandan A. Novel synthesis of spinel Mn x Co 1− x Al 2 O 4 (x= 0.0 to 1.0) nanocatalysts: effect of Mn 2+ doping on structural, morphological, and opto-magnetic properties. J Supercond Nov Magnetism 2017;30:691–9.
[2] Loharkar PK, Ingle A, Jhavar S. Parametric review of microwave-based materials processing and its applications. J Mater Res Technol 2019;8:3306–26.
[3] Abutarboush HF, Shamim A. Based inkjet-printed tri-band U-slot monopole antenna for wireless applications. IEEE Antenn Wireless Propag Lett 2012;11:1234–7.
[4] Rahman MA, Islam MT, Singh MSJ, Samsuzzaman M, Chowdhury ME. Synthesis and characterization of Mg–Zn ferrite based flexible microwave composites and its application as SNG metamaterial. Sci Rep 2021;11:1–14.
[5] Abouzir E, Belaiche M, Elansary M, Ahmani Ferdi C, Bsoul I. Novel magnetic nanomaterial Co0. 7Zn0. 3Fe2− xGdxO4 for nanotechnology applications: experimental and theoretical investigations. J Mater Sci Mater Electron 2021:1–18.
[6] Hazra S, Ghosh N. Preparation of nanoferrites and their applications. J Nanosci Nanotechnol 2014;14:1983–2000.
[7] Algarou N, Slimani Y, Almessiere M, Alahmari F, Vakhitov M, Klygach D, et al. Magnetic and microwave properties of SrFe12O19/MCe0. 04Fe1. 96O4 (M= Cu, Ni, Mn, Co and Zn) hard/soft nanocomposites. J Mater Res Technol 2020;9:5858–70.
[8] Song F, Shen X, Liu M, Xiang J. Preparation and magnetic properties of SrFe12O19/Ni0. 5Zn0. 5Fe2O4 nanocomposite ferrite microfibers via sol–gel process. Mater Chem Phys 2011;126:791–6.
[9] Tatarchuk T, Myslin M, Mironyuk I, Bououdina M, Pędziwiatr AT, Gargula R, et al. Synthesis, morphology, crystallite size and adsorption properties of nanostructured Mg–Zn ferrites with enhanced porous structure. J Alloys Compd 2020;819:152945.
[10] Trukhanov A, Astapovich K, Turchenko V, Almessiere M, Slimani Y, Baykal A, et al. Influence of the dysprosium ions on structure, magnetic characteristics and origin of the reflection losses in the Ni–Co spinels. J Alloys Compd 2020;841:155667.
[11] Almessiere MA, Slimani Y, GüngüneŞ H, Korkmaz AD, Zubar T, Trukhanov S, et al. Influence of Dy3+ ions on the microstructures and magnetic, electrical, and microwave properties of [Ni0. 4Cu0. 2Zn0. 4](Fe2−x Dy x) O4 (0.00≤ x≤ 0.04) spinel ferrites. ACS Omega 2021;6:10266–80.
[12] Sukhija S, Sarin RK. A U-shaped meandered slot antenna for biomedical applications. Prog Electromagn Res M 2017;62:65–77.
[13] Motevasselian A, Whittow WG. Patch size reduction of rectangular microstrip antennas by means of a cuboid ridge. IET Microw, Antennas Propag 2015;9:1727–32.
[14] Wakrim L, Ibnyaich S, Hassani MMr. The study of the ground plane effect on a Multiband PIFA Antenna by using genetic Algorithm and Particle swarm optimization. J Microw Optoelectron Electromagn Appl 2016;15:293–308.
[15] Su Z, Chang H, Wang X, Sokolov AS, Hu B, Chen Y, et al. Low loss factor Co2Z ferrite composites with equivalent permittivity and permeability for ultra-high frequency applications. Appl Phys Lett 2014;105:062402.
[16] Azim R, Islam MT, Misran N. Ground modified double-sided printed compact UWB antenna. Electron Lett 2011;47:9–10.
[17] Rahman MA, Islam MT, Singh MSJ, Samsuzzaman M. Polarization-independent multiband double-negative metamaterial through ferrite-based flexible substrate with

tunable microwave dielectric properties. Results Phys 2021;25:104214.
[18] Misran N, Yusop SH, Islam MT, Ismail MY. Analysis of parameterization substrate thickness and permittivity for concentric split ring square reflectarray element. Jurnal Kejuruteraan (J Eng) 2012;23:11–6.
[19] Vinnik D, Zhivulin V, Sherstyuk D, Starikov AY, Zezyulina P, Gudkova S, et al. Electromagnetic properties of zinc–nickel ferrites in the frequency range of 0.05–10 GHz. Mater Today Chem 2021;20:100460.
[20] Vinnik D, Zhivulin V, Sherstyuk D, Starikov AY, Zezyulina P, Gudkova S, et al. Ni substitution effect on the structure, magnetization, resistivity and permeability of zinc ferrites. J Mater Chem C 2021;9:5425–36.
[21] Islam MT, Rahman MA, Singh MJ, Hossain I, Soliman MS, Almalki SH, et al. Structural, dielectric, and magnetic properties characterization of sol-gel synthesized CaxZn (0.90-x) Ni0. 10Fe2O4 nanopowder and its application as flexible microwave substrate with polarization-insensitive SNG metamaterial. J Mater Res Technol 2022;18:5226–37.
[22] Trukhanov A, Turchenko V, Bobrikov I, Trukhanov S, Kazakevich I, Balagurov A. Crystal structure and magnetic properties of the BaFe12− xAlxO19 (x= 0.1–1.2) solid solutions. J Magn Magn Mater 2015;393:253–9.
[23] Trukhanov S, Trukhanov A, Turchenko V, Trukhanov AV, Trukhanova E, Tishkevich D, et al. Polarization origin and iron positions in indium doped barium hexaferrites. Ceram Int 2018;44:290–300.
[24] Huitema L, Reveyrand T, Mattei J-L, Arnaud E, Decroze C, Monediere T. Frequency tunable antenna using a magneto-dielectric material for DVB-H application. IEEE Trans Antenn Propag 2013;61:4456–66.
[25] Rahman MA, Ahamed E, Faruque MRI, Islam MT. Preparation of NiAl 2 O 4-based flexible substrates for metamaterials with negative dielectric properties. Sci Rep 2018;8:1–13.
[26] Vrba D, Rodrigues D, Vrba J, Stauffer PR. Metamaterial antenna arrays for improved uniformity of microwave hyperthermia treatments. Prog Electromagn Res 2016;156:1–12.
[27] Guo J, Li X, Chen Z, Zhu J, Mai X, Wei R, et al. Magnetic NiFe2O4/Polypyrrole nanocomposites with enhanced electromagnetic wave absorption. J Mater Sci Technol 10 May 2022;108:64–72.
[28] Rahman MA, Islam MT, Singh MJ, Hossain I, Rmili H, Samsuzzaman M. Magnetic, dielectric and structural properties of CoxZn (0.90-x) Al0. 10Fe2O4 synthesized by sol–gel method with application as flexible microwave substrates for microstrip patch antenna. J Mater Res Technol 2022;16:934–43.
[29] Abdulkarim YI, Awl HN, Alkurt FO, Muhammadsharif FF, Saeed SR, Karaaslan M, et al. A thermally stable and polarization insensitive square-shaped water metamaterial with ultra-broadband absorption. J Mater Res Technol 2021;13:1150–8.
[30] Bhongale S. Mg-Nd-Cd ferrite as substrate for X-band microstrip patch antenna. J Magn Magn Mater 2020;499:165918.
[31] Almessiere MA, Güner S, Slimani Y, Hassan M, Baykal A, Gondal MA, et al. Structural and magnetic properties of Co0. 5Ni0. 5Ga0. 01Gd0. 01Fe1. 98O4/ZnFe2O4 spinel ferrite nanocomposites: comparative study between sol-gel and pulsed laser ablation in liquid approaches. Nanomaterials 2021;11:2461.
[32] Almessiere M, Algarou N, Slimani Y, Sadaqat A, Baykal A, Manikandan A, et al. Investigation of exchange coupling and microwave properties of hard/soft (SrNi0. 02Zr0. 01Fe11. 96O19)/(CoFe2O4) x nanocomposites. Mater Today Nano 2022;18:100186.
[33] Saxena NK, Singh B, Kumar N, Pourush P. Microstrip triangular patch antenna fabricated on LiTiZn ferrite substrate and tested in the X band range. AEU-Int J Electron Commun 2012;66:140–2.
[34] Su H, Tang X, Zhang H, Jing Y, Bai F, Zhong Z. Low-loss NiCuZn ferrite with matching permeability and permittivity by two-step sintering process. J Appl Phys 2013;113:17B301.
[35] Borah K, Phukan A, Bhattacharyya S, Bhattacharyya NS. Design of light weight microstrip patch antenna on dielectric and magnetodielectric substrate for broadband applications in X-Band. Prog Electromagn Res B 2014;60:157–68.
[36] Naidu V, Ahamed Kandu Sahib S, Sivabharathy M, Legadevi R, Senthil Kumar A, Prakash C, et al. Synthesis and characterization of novel nanoceramic magnesium ferrite material doped with samarium and dysprosium for designing–microstrip patch antenna. In: Defect and diffusion forum; 2012. p. 35–50.
[37] Dukenbayev K, Korolkov IV, Tishkevich DI, Kozlovskiy AL, Trukhanov SV, Gorin YG, et al. Fe3O4 nanoparticles for complex targeted delivery and boron neutron capture therapy. Nanomaterials 2019;9:494.
[38] Tishkevich D, Korolkov I, Kozlovskiy A, Anisovich M, Vinnik D, Ermekova A, et al. Immobilization of boron-rich compound on Fe3O4 nanoparticles: stability and cytotoxicity. J Alloys Compd 2019;797:573–81.
[39] Almessiere MA, Trukhanov AV, Slimani Y, You K, Trukhanov SV, Trukhanova EL, et al. Correlation between composition and electrodynamics properties in nanocomposites based on hard/soft ferrimagnetics with strong exchange coupling. Nanomaterials 2019;9:202.
[40] Almessiere MA, Slimani Y, Algarou NA, Vakhitov MG, Klygach DS, Baykal A, et al. Tuning the structure, magnetic, and high frequency properties of Sc-doped Sr0. 5Ba0. 5ScxFe12-xO19/NiFe2O4 hard/soft nanocomposites. Adv Electron Mater 2022;8:2101124.
[41] Adamson EB, Ludwig KD, Mummy DG, Fain SB. Magnetic resonance imaging with hyperpolarized agents: methods and applications. Phys Med Biol 2017;62:R81.
[42] Ahmad HA, Yu HJ, Miller CG. Medical imaging modalities. In: Medical imaging in clinical trials. Springer; 2014. p. 3–26.
[43] Frangi AF, Tsaftaris SA, Prince JL. Simulation and synthesis in medical imaging. IEEE Trans Med Imag 2018;37:673–9.
[44] Tariq M, Siddiqi AA, Narejo GB, Andleeb S. A cross sectional study of tumors using bio-medical imaging modalities. Curr Med Imag 2019;15:66–73.
[45] Cazzato RL, Garnon J, Shaygi B, Koch G, Tsoumakidou G, Caudrelier J, et al. PET/CT-guided interventions: indications, advantages, disadvantages and the state of the art. Minim Invasive Ther Allied Technol 2018;27:27–32.
[46] Chakraborty S, Chatterjee S, Ashour AS, Mali K, Dey N. Intelligent computing in medical imaging: a study. In: Advancements in applied metaheuristic computing. IGI global; 2018. p. 143–63.
[47] Chew KM, Yong CY, Sudirman R, Wei STC. Bio-signal processing and 2D representation for brain tumor detection using microwave signal analysis. In: 2018 IEEE symposium on computer applications & industrial electronics (ISCAIE); 2018. p. 303–9.
[48] Dougeni E, Faulkner K, Panayiotakis G. A review of patient dose and optimisation methods in adult and paediatric CT scanning. Eur J Radiol 2012;81:e665–83.
[49] Jacobs MA, Ibrahim TS, Ouwerkerk R. MR imaging: brief overview and emerging applications. Radiographics 2007;27:1213–29.
[50] Jones KM, Michel KA, Bankson JA, Fuller CD, Klopp AH, Venkatesan AM. Emerging magnetic resonance imaging technologies for radiation therapy planning and response assessment. Int J Radiat Oncol Biol Phys 2018;101:1046–56.

[51] Alqadami AS, Bialkowski KS, Mobashsher AT, Abbosh AM. Wearable electromagnetic head imaging system using flexible wideband antenna array based on polymer technology for brain stroke diagnosis. IEEE Trans Biomed Circuits Syst 2018;13:124–34.

[52] Hossain A, Islam MT, Islam M, Chowdhury ME, Rmili H, Samsuzzaman M. A planar ultrawideband patch antenna array for microwave breast tumor detection. Materials 2020;13:4918.

[53] Hossain A, Islam MT, Islam MS, Chowdhury ME, Almutairi AF, Razouqi QA, et al. A YOLOv3 deep neural network model to detect brain tumor in portable electromagnetic imaging system. IEEE Access 2021;9:82647–60.

[54] Islam MS, Islam MT, Hoque A, Islam MT, Amin N, Chowdhury ME. A portable electromagnetic head imaging system using metamaterial loaded compact directional 3D antenna. IEEE Access 2021;9:50893–906.

[55] Mobashsher A, Bialkowski K, Abbosh A, Crozier S. Design and experimental evaluation of a non-invasive microwave head imaging system for intracranial haemorrhage detection. PLoS One 2016;11:e0152351.

[56] Mobashsher AT, Abbosh AM, Wang Y. Microwave system to detect traumatic brain injuries using compact unidirectional antenna and wideband transceiver with verification on realistic head phantom. IEEE Trans Microw Theor Tech 2014;62:1826–36.

[57] Trukhanov S, Lobanovski L, Bushinsky M, Fedotova V, Troyanchuk I, Trukhanov A, et al. Study of A-site ordered PrBaMn2O6− δ manganite properties depending on the treatment conditions. J Phys Condens Matter 2005;17:6495.

[58] Trukhanov S, Trukhanov A, Stepin S, Szymczak H, Botez C. Effect of the size factor on the magnetic properties of manganite La0. 50Ba0. 50MnO3. Phys Solid State 2008;50:886–93.

[59] Turchenko V, Trukhanov S, Kostishin V, Damay F, Porcher F, Klygach D, et al. Features of structure, magnetic state and electrodynamic performance of SrFe12− xInxO19. Sci Rep 2021;11:1–14.

[60] Turchenko VA, Trukhanov SV, Kostishin VGe, Damay F, Porcher F, Klygach DS, et al. Impact of In3+ cations on structure and electromagnetic state of M− type hexaferrites. J Energy Chem 2022;69:667–76.

[61] Lin Y, Liu X, Yang H, Wang F, Liu C. Magnetic and dielectric properties of laminated Ca (Zn1/3Nb2/3) O3-Ni0. 8Zn0. 2Fe2O4 magneto-dielectric composites. Mater Res Bull 2017;86:101–6.

[62] Koops C. On the dispersion of resistivity and dielectric constant of some semiconductors at audio frequencies. Phys Rev 1951;83:121.

[63] Wagner KW. Zur theorie der unvollkommenen dielektrika. Ann Phys 1913;345:817–55.

[64] Trukhanov S, Troyanchuk I, Pushkarev N, Szymczak H. The influence of oxygen deficiency on the magnetic and electric properties of La0. 70Ba0. 30MnO3− γ (0≤ γ≤ 0.30) manganite with a perovskite structure. J Exp Theor Phys 2002;95:308–15.

[65] Trukhanov S, Trukhanov A, Vasiliev A, Balagurov A, Szymczak H. Magnetic state of the structural separated anion-deficient La0. 70Sr0. 30MnO2. 85 manganite. J Exp Theor Phys 2011;113:819–25.

[66] Saini A, Thakur A, Thakur P. Matching permeability and permittivity of Ni 0.5 Zn 0.3 Co 0.2 in 0.1 Fe 1.9 O 4 ferrite for substrate of large bandwidth miniaturized antenna. J Mater Sci Mater Electron 2016;27:2816–23.

[67] Narang SB, Pubby K. Single-layer & double-layer microwave absorbers based on Co–Ti substituted barium hexaferrites for application in X and Ku-band. J Mater Res 2016;31:3682–93.

[68] Mobashsher A, Abbosh A. Three-dimensional human head phantom with realistic electrical properties and anatomy. IEEE Antenn Wireless Propag Lett 2014;13:1401–4.

[69] Islam MT, Samsuzzaman M, Kibria S, Misran N, Islam MT. Metasurface loaded high gain antenna based microwave imaging using iteratively corrected delay multiply and sum algorithm. Sci Rep 2019;9:1–14.